# A Hyperthermophilic Plant-Type [2Fe-2S] Ferredoxin from *Aquifex aeolicus* Is Stabilized by a Disulfide Bond†

Jacques Meyer,*,‡ Michael D. Clay,§ Michael K. Johnson,§ Audria Stubna,|| Eckard Münck,|| Catherine Higgins,⊥ and Pernilla Wittung-Stafshede⊥

*Département de Biologie Moléculaire et Structurale, CEA-Grenoble, 38054 Grenoble, France, Department of Chemistry and Center for Metalloenzyme Studies, University of Georgia, Athens, Georgia 30602, Department of Chemistry, Carnegie Mellon University, Pittsburgh, Pennsylvania 15213, and Chemistry Department, Tulane University, New Orleans, Louisiana 70118*

*Received November 27, 2001; Revised Manuscript Received January 11, 2002*

ABSTRACT: A [2Fe-2S] ferredoxin (Fd1) from the hyperthermophilic bacterium *Aquifex aeolicus* has been obtained by heterologous expression of the encoding gene in *Escherichia coli*. Sequence comparisons show that this protein belongs to the extended family of plant- and mammalian-type [2Fe-2S] ferredoxins but also indicate that it is not closely similar to either the plant-type or mammalian-type subfamilies. Instead, it appears to bear some similarity to novel members of this family, in particular the Isc-type ferredoxins involved in the assembly of iron−sulfur clusters in vivo. The two redox levels of the [2Fe-2S]$^{2+/+}$ metal site of *A. aeolicus* ferredoxin have been studied by UV−visible, resonance Raman, EPR, variable temperature magnetic circular dichroism, and Mössbauer spectroscopies. A full-spin Hamiltonian analysis is given for the Mössbauer spectra. In aggregate, the spectroscopic data reveal differences with both the plant-type and mammalian-type ferredoxins, in keeping with the sequence comparisons. The midpoint potential of the [2Fe-2S]$^{2+/+}$ couple, at −375 mV versus the normal hydrogen electrode, is more negative than those of mammalian-type ferredoxins and at the upper end of the range covered by plant-type ferredoxins. *A. aeolicus* ferredoxin contains two cysteines in addition to the four that are committed as ligands of the [2Fe-2S] cluster. These two residues have been shown by chemical modification and site-directed mutagenesis to form a disulfide bridge in the native protein. While that cystine unit plays a significant role in the exceptional thermostability of *A. aeolicus* ferredoxin ($T_m$ = 121 °C at pH 7 versus $T_m$ = 113 °C in a molecular variant where the disulfide bridge has been removed), it does not bear on the properties of the [2Fe-2S]$^{2+/+}$ chromophore. This observation is consistent with the large distance (ca. 20 Å) that is predicted to separate the iron−sulfur chromophore from the disulfide bridge.

Ferredoxins (Fds)[1] are small iron−sulfur (Fe-S) proteins that contain either [4Fe-4S]/[3Fe-4S] or [2Fe-2S] clusters (*1*, *2*). While a few among the latter constitute a novel class of thioredoxin-like Fds (*3*, *4*), their vast majority belongs to a monophyletic group known as plant- and mammalian-type Fds, which consists of two main subgroups. The first of these includes Fds transferring electrons from photosystem I to several Fd-dependent enzymes in plants, algae, and cyanobacteria (*5*). Fds of the second subgroup participate in electron transfer chains linked to hydroxylation reactions, not only in mammals [e.g., adrenodoxin (Adx)] but also in a variety of other organisms including bacteria [e.g., putidaredoxin] (*6*). Evidence for a novel function has recently been reported for some Adx-like Fds, namely, their involvement in the assembly of iron−sulfur clusters in vivo (*7*−*9*). Some of these Fds are most similar to Adx [hence the name Yah1p (for *y*east *a*drenodoxin *h*omologue) given to one member of this group (*10*)], but many display less well-defined relationships.

A remarkable feature of [2Fe-2S] plant- and mammalian-type Fds is their sparse distribution among extremophiles. While halophilic archaea contain such Fds (*11*), there is no evidence that any hyperthermophilic archaeon might do so. As a typical example, the genome of the hyperthermophilic sulfate-reducing archaeon *Archaeoglobus fulgidus* includes at least eight genes potentially encoding [3Fe-4S]/[4Fe-4S] Fds but not a single one for plant- and mammalian-type [2Fe-2S] Fds (*12*). In fact, the only hyperthermophile that is known to contain at least one plant- and mammalian-type [2Fe-2S] Fd is the bacterium *Aquifex aeolicus* (*13*, *14*). This protein has been the subject of a short report (*14*) and is endowed

† This research was supported by the National Institutes of Health (Grants GM59663 to P.W.-S. and GM62524 to M.K.J.) and the National Science Foundation (Grant MCD-9416224 to E.M.). P.W.-S. is an Alfred P. Sloan Research Fellow.

* To whom correspondence should be addressed: DBMS-BECP, CEA-Grenoble, 38054 Grenoble, France. Tel: (33) 4 38 78 44 23. Fax: (33) 4 38 78 98 08. E-mail: jacques.meyer@cea.fr.

‡ CEA-Grenoble.

§ University of Georgia.

|| Carnegie Mellon University.

⊥ Tulane University.

[1] Abbreviations: *Aae*, *Aquifex aeolicus*; Adx, adrenodoxin; CD, circular dichroism; DTNB, 5,5′-dithiobis(2-nitrobenzoic acid); TNB, 5-thio-2-nitrobenzoate; DTT, dithiothreitol; ENDOR, electron−nuclear double resonance; EPR, electron paramagnetic resonance; Fd, ferredoxin; GuHCl, guanidine hydrochloride; I-AEDANS, *N*-iodoacetyl-*N*′-(5-sulfo-1-naphthyl)ethylenediamine; VTMCD, variable temperature magnetic circular dichroism; SDS, sodium dodecyl sulfate; PAGE, polyacrylamide electrophoresis; PCR, polymerase chain reaction; RR, resonance Raman; WT, wild type.

10.1021/bi015981m CCC: $22.00 
Published on Web 02/06/2002

with at least two interesting peculiarities: its sequence places it in the twilight zone between plant-type and mammalian-type Fds, and it is the only hyperthermophilic member of this class of proteins. We have therefore carried out and report here an investigation of its biochemical and spectroscopic properties.

## MATERIALS AND METHODS

Enzymes were purchased from Roche Molecular Biochemicals. Oligonucleotides and culture media were from Life Technologies (Cergy-Pontoise, France). Guanidine hydrochloride (GuHCl), of highest purity, was purchased from Sigma. Polymerase chain reactions (PCR) were run on a Perkin-Elmer 2400 machine. Plasmid DNA was purified with the EasyPrep kit (Pharmacia). DNA sequencing was performed by Genome Express (Meylan, France).

*Gene Cloning and Protein Purification.* All common DNA manipulations were as described (*15*). The gene encoding Fd1 [orf 919a (*13*)] was lifted from *A. aeolicus* genomic DNA (gift from Dr. R. Huber, University of Regensburg, Germany) by PCR using the following primers. The N-terminal primer hybridized to the noncoding strand: 5′ cttttgcttagaatacttg*cat*ATGaag 3′ (*Nde*I restriction site in italics, ATG start codon in upper case). The C-terminal primer hybridized to the coding strand: 5′ ctacataaagg*aagctt*cTTAatc 3′ (*Hin*dIII restriction site in italics, stop codon in upper case). After a DNA denaturation step of 5 min at 94 °C, *Pwo* DNA polymerase and the deoxynucleotide mix were added, and 25 cycles of amplification (30 s at 94 °C, 30 s at 50 °C, 2 min at 72 °C) were performed, followed by a 7 min elongation step. The amplified DNA fragment was extracted with phenol/chloroform, precipitated with ethanol, digested with *Hin*dIII and *Nde*I, purified by electrophoresis through a low-melting agarose gel, and ligated into the pT7-7 vector (*16*) digested with the same restriction enzymes. The ligation mixture was used to transform *Escherichia coli* DH5α cells. Clones containing the Fd1-encoding gene were sequenced and found to match perfectly the corresponding part of the *A. aeolicus* genome sequence (*13*). The Fd1-encoding gene was expressed in *E. coli* K38 cells using the pT7-7 and pGP1-2 double plasmid system (*16*) as described previously for the [2Fe-2S] *Clostridium pasteurianum* Fd (*17*). Cells from a 10 L culture in minimal medium (M9 from Life Technologies, complemented with 0.2% glucose, 1 mM $MgSO_4$, 25 μM iron citrate, 0.5 mg/L vitamin B1, 100 mg/L ampicillin, 50 mg/L kanamycin) were resuspended in 250 mL of Tris-HCl, 50 mM, pH 8.0, disrupted by sonication (3 × 1 min at 300 W), and centrifuged for 30 min at 35000*g*. The supernatant was heated to 65 °C for 10 min, kept at 0 °C for another 10 min, and centrifuged (35000*g*, 30 min) to remove the denatured *E. coli* proteins. The dark red supernatant was loaded on a 2 × 7 cm DE-52 (Whatman) column equilibrated with Tris-HCl, 50 mM, pH 8.0. From this step on, the purification was carried out under argon. The DE52 column was washed with Tris-HCl, 50 mM, pH 8.0, containing stepwise incremented concentrations of NaCl (0.05, 0.1, 0.2, 0.25, 0.3 M). The Fd was eluted with 0.3 M NaCl, concentrated in an Amicon cell fitted with a PM10 membrane, and loaded on a 1.5 × 100 cm Superdex-75 (Pharmacia) column equilibrated with Tris-HCl, 20 mM, pH 8.0, and NaCl, 0.2 M. The last purification step was an HPLC chromatography on a PL-SAX (Polymer Labs) anion-exchange column developed with a 0−0.4 M NaCl gradient in Tris-HCl, 0.01 M, pH 8.0. *A. aeolicus* Fd1 (*Aae* Fd1) displayed the characteristic reddish brown color of [2Fe-2S] proteins. Its purification was monitored by SDS−PAGE electrophoresis (not shown) and by the increase of the $A_{420}/A_{280}$ ratio (see Results).

The Cys87Ala (C87A) variant of *Aae* Fd1 was prepared by a procedure involving two rounds of PCR to create a mutation and amplify a DNA fragment surrounding it (*18*). The mutagenic oligonucleotide, 5′ gaaaaagaagacGCcgacgaaatagtg 3′ (mutated bases in upper case), was designed to hybridize to the noncoding strand. Cloning and expression of the mutated gene were as for the wild-type (WT) one. The C87A Fd1 was purified as described for the WT, but the duration of the heat treatment (65 °C) was reduced to 3 min.

The samples of human [2Fe-2S] ferredoxin (adrenodoxin) and *Anabaena* 7120 vegetative [2Fe-2S] ferredoxin for comparative spectroscopic studies were supplied by Professor John L. Markley (University of Wisconsin) (*19*).

*Modification of Cysteine Residues*. Alkylation of free thiols with the fluorescent reagent I-AEDANS (Sigma) was performed as described (*20*). Proteins and all reagents were in Tris-HCl, 0.5 M, pH 8. The reactions were initiated by adding 10 μL of a 10 mM I-AEDANS solution to 20 μL of a 50 μM Fd solution. After 30 s (results were unchanged when the incubation time was varied over a 20−120 s range) the alkylation reaction was stopped by addition of 10 μL of a 1 M DTT solution. In control experiments DTT was added first and I-AEDANS 30 s later. For reduction of the putative disulfide bond, the protein (50 μM) was preincubated for 30 min in the presence of DTT (0.5 mM), and the alkylation reaction was then carried out as above. The reaction products were analyzed by SDS−PAGE (*21*). Protein alkylation was observed by UV illumination of the gel prior to staining with Coomassie blue R-250. Thiol alkylation by DTNB (Sigma) was monitored by following the appearance of the TNB [$\epsilon_{412}$ = 13600 $M^{-1}$ $cm^{-1}$ (*22*)] anion released upon reaction of DTNB with free thiols.

*Redox Potentials*. Redox potentials were measured in an oxygen-free (2 ppm) glovebox at 20 °C by reductive and oxidative titrations with dithionite and ferricyanide, respectively, as described (*18*, *23*). The reaction medium (2.3 mL) contained 50 mM Tris-HCl, pH 8.0, 0.2 M NaCl, 0.08 mM Fd, and the mediators safranine T (Fluka), benzyl viologen (Serva), and methyl viologen (Serva), each at a concentration of 2.5 μM. UV−visible absorption spectra were recorded in the 350−800 nm range, and the absorbance at 420 nm, where the contribution of the mediators is negligible, was used for the calculations. The potential was measured between the platinum electrode and the Ag/AgCl reference electrode of a combined electrode.

*Spectroscopic Methods*. UV−visible absorption spectra were recorded on Hewlett-Packard 8452 or 8453 diode array spectrophotometers. VTMCD spectra were recorded using Oxford Instruments SM3 or Spectromag 4000 split-coil superconducting magnets (1.5−300 K and 0−7 T) mated to a Jasco J-500C spectropolarimeter. The samples used for VTMCD contained 50% (v/v) ethylene glycol in order to form an optically transparent glass on freezing. The experimental protocols used in VTMCD studies, namely, accurate

temperature and magnetic field measurements, anaerobic sample handling, and assessment of residual strain in the frozen samples, have been described in detail elsewhere (*24*, *25*). X-band EPR spectra were recorded on a Brüker ESP-300E EPR spectrometer fitted with an Oxford Instruments ESR-9 liquid helium flow cryostat. Resonance Raman spectra were recorded using an Instruments SA Ramanor U1000 spectrometer fitted with a cooled RCA 31034 photomultiplier tube with a 90° scattering geometry. Spectra were recorded digitally using photon-counting electronics. Multiple scans (20−50) were collected and averaged in order to increase the signal to noise ratio. Band positions were calibrated using the excitation frequency and a $CCl_4$ standard and are accurate to within $\pm 1$ cm$^{-1}$. Lines from a Coherent Innova 100 10-W argon ion laser were used in this work, and plasma lines were removed using a Pellin-Broca prism premonochromator. Scattering was collected from the surface of a frozen 10 $\mu$L drop of sample using a custom-designed anaerobic sample cell (*26*) attached to the coldfinger of an Air Products Displex Model CSA-202E closed cycle refrigerator. The Mössbauer spectra were collected on a constant acceleration spectrometer, using two cryostats that allowed studies in applied fields up to 8.0 T between 1.5 K and room temperature. Isomer shifts are quoted relative to Fe metal at 298 K. Spectral simulations were generated with the WMOSS software package (WEB Research, Edina, MN). Cultures for the preparation of $^{57}$Fe-enriched *Aae* Fd1 were as described (*14*).

*Chemically Induced Unfolding*. GuHCl was used to promote *Aae* Fd1 (WT and C87A) unfolding at 20 °C, at pH 10.0, 7.0, and 2.5. Titrations were performed with 10−20 $\mu$M Fd1 in phosphate (pH 7) or glycine (pH 2.5 and 10) buffers (concentration 20 mM). Samples were incubated for various lengths of time (from 1 to 116 h; see Table 2) before spectroscopic measurements. Unfolding was probed by far-UV CD (200−300 nm) on a JASCO-820 instrument, by visible absorption (300−700 nm) on a Cary-50 spectrophotometer, and by tryptophan emission (300−450 nm, excitation at 280 nm) on a Varian Eclipse instrument. The transition midpoint ($[GuHCl]_{1/2}$) at each solution condition (pH, incubation time, WT or C87A Fd1) was obtained by direct inspection of the data.

*Thermally Induced Unfolding.* Thermally induced unfolding of Fd1 was monitored by visible absorption at 418 nm in various pH/GuHCl conditions. The absorption signal from ~15 $\mu$M ferredoxin was recorded, one data point collected per second, with 2 min/deg, 4 min/deg, or 8 min/deg scan rates from 20 to 95 °C. The thermal reactions were monitored on a Cary-100 spectrophotometer. In the end, the temperature was decreased to 20 °C and a spectrum recorded to check for refolding. The thermal midpoint ($T_m$) at each GuHCl concentration was determined by direct inspection of the transition.

## RESULTS

*Purification*. Since *Aae* Fd1 is very thermostable (see below), a thermal treatment of the *E. coli* cell extracts has been implemented as previously described for *A. aeolicus* Fd4 (*27*) in order to eliminate most of the *E. coli* proteins. *Aae* Fd1 is also very acidic (calculated p$I$ = 4.2), and therefore anion-exchange chromatography proved to be a very efficient purification step. Purification, as monitored by SDS−PAGE (not shown) and UV−visible absorption spectroscopy, was satisfactory after the gel filtration in most cases. Otherwise, a final anion-exchange HPLC step was included in the purification procedure.

*Amino Acid Sequence Comparisons*. The amino acid sequence of *Aae* Fd1 consists of 96 residues and displays the characteristics of plant- and mammalian-type Fds. It has therefore been compared with sequences of representative members of this family (Figure 1). The alignment is consistent with a recent structural alignment proposed for a lesser number of plant-type and Adx-like Fds (*6*). All proteins included in Figure 1 are homologous, but their wide distribution and functional diversity have resulted in a low overall sequence conservation. In fact, only five residues, including the four cysteine ligands of the [2Fe-2S] cluster, are fully conserved. Several of these proteins contain cysteine residues in addition to the four cluster ligands. Such is the case of *Aae* Fd1, which has two additional cysteines in positions 52 and 87 (Figure 1).

Inspection of the alignment of Figure 1 reveals that the sequence of *Aae* Fd1 is related to Adx-like sequences by some of its features, while others are more reminiscent of plant-type Fds. This is illustrated in the dendrogram (Figure 2) which represents graphically the similarities of the sequences aligned in Figure 1. The main groups, those of photosynthesis-linked Fds and Adx-like Fds, are clearly separated in the dendrogram. Fds involved in photosynthesis (upper part of Figure 2) constitute the most homogeneous group, but they are nevertheless split into plant and cyanobacterial subtrees (*5*). Halophilic archaeal Fds may be considered as distinct from the plant-type Fds (*11*) but are their closest relatives. Fds related to Adx (lower part of Figure 2) are far more diverse than those involved in photosynthesis. At least three subtrees, each having relatively long branches, are prominent. The two most homogeneous ones are those of bacterial Fds involved in Fe-S cluster assembly (Isc-Fds) (*7*, *9*) and the putidaredoxin group. The subtree of eukaryotic Adx-like sequences includes proteins involved in hydroxylation electron transfer chains (Adx itself), as well as others involved in Fe-S cluster assembly (Yah1p). A few other [2Fe-2S] Fds, including *Aae* Fd1, are located in a twilight zone between plant-type and Adx-like Fds. They are not only outside of the main groups but also quite apart from each other. This indicates sequence idiosyncrasies that are likely to be for the most part reflections of their atypical functions. For instance, XylT specifically reactivates oxygen-inactivated oxygenases (*30*), while *Rhodobacter capsulatus* FdIV is somehow involved in dinitrogen fixation (*31*). Another unique Fd from *R. capsulatus*, FdV (*32*), also maps in this region (not shown). The function of *Aae* Fd1 is unknown, but its closest relatives, apart from *R. capsulatus* FdIV, are the bacterial Isc-Fds.

*Spectroscopy*. UV−visible absorption spectra of as-isolated *Aae* Fd1 display bands at ca. 550, 460, 420, and 340 nm (Figure 3) that collectively are characteristic of $[2Fe\text{-}2S]^{2+}$ clusters. The relatively red-shifted 346 nm band, with a shoulder on its high energy side, and the very broad shoulder in the 500−560 nm region are reminiscent of spectra of XylT (*30*), *R. capsulatus* FdIV (*33*), and FdV (*32*). Since *Aae* Fd1 contains no tyrosine and a single tryptophan (W65), the UV absorbance of the polypeptide chain is relatively low

```
6              ATFKVTLINEAEGT------KHEIEVPDDEYILDAAEE-QGYDLPFS---CRAG-ACSTCAGKLVSGT-- 57
7              ATYKVTLINEAEGI------NETIDCDDDTYILDAAEE-AGLDLPYS---CRAG-ACSTCAGTITSGT-- 57
9              ATYKVTLV-RPDGS------ETTIDVPEDEYILDVAEE-QGLDLPFS---CRAG-ACSTCAGKLLEGE-- 56
8              ASYTVKLI-TPDG-------ESSIECSDDTYILDAAEE-AGLDLPYS---CRAG-ACSTCAGKITAGS-- 55
4              ATYKVKLV-TPQG-------QQEFDCPDDVYILDQAEE-EGIDLPYS---CRAG-SCSSCAGKVKQGE-- 55
5              ATYKVKLV-TPDG-------PVEFNCPDDVYILDQAEE-EGHDLPYS---CRAG-SCSSCAGKVTAGT-- 55
1               AYKVTLV-TPTG-------NVEFQCPDDVYILDAAEE-EGIDLPYS---CRAG-SCSSCAGKLKTGS-- 54
2              ATYNVKLI-TPDG-------EVEFKCDDDVYVLDQAEE-EGIDIPYS---CRAG-SCSSCAGKVVSGS-- 55
3              ATYNVKLI-TPEG-------EVELQVPDDVYILDFAEE-EGIDLPFS---CRAG-SCSSCAGKVVSGS-- 55
10           17-DMYDDDVFGEASDMDLDDEDYGSLEVNEGEYILEAAEA-QGYDWPFS---CRAG-ACANCAAIVLEGD-- 79
14                AKITYIQHDG------AEQVIDVKPGLTVMEGAVK-NNVPGIDA--DCGGACACATCHVYVDEAWLD 58
15               MTKLTFIAHDG------TQFDVDAENGSTVMENAIR-NAVPGIEA--ECGGACACATCHVYVDEAWTA 59
13                AKIIFIEHNG------TRHEVEAKPGLTVMEAARD-NGVPGIDA--DCGGACACSTCHAYVDPAWVD 58
12               MSKVVYVSHDG------TRRELDVADGVSLMQAAVS-NGIYDIVG--DCGGSASCATCHVYVNEAFTD 59
16           SSSEDKITVHFINRDG------ETLTTKGKIGDSLLDVVVQ-NNLD-IDGFGACEGTLACSTCHLIFEQHIFE 65
17           SSSEDKITVHFINRDG------ETLTTKGKVGDSLLDVVVE-NNLD-IDGFGACEGTLACSTCHLIFEDHIYE 65
18        55-PKPGEELKITFILKDG------SQKTYEVCEGETILDIAQG-HNLD-MEG--ACGGSCACSTCHVIVDPDYYD 117
19                                                          MEG--ACEASLACTTCHVYVQHDYLQ 24
23             MPQIVILPHADHCP------EGAVFEAKPGETILDAALR-NGIEIEHA---CEKSCACTTCHVIVREGL-D 60
22            MMPQIVFLPHEVHCP------EGRVVEAETGESILEAALR-NDIEIEHA---CEMSCACTTCHVIVRDGF-D 61
21             MPKIVILPHQDLCP------DGAVLEANSGETILDAALR-NGIEIEHA---CEKSCACTTCHCIVREGF-D 60
20             MPKVLFLPHKILLP------KSIECEAQTGETILTVALR-NNIKLEHA---CEQSCACSTCHCIIKKGF-F 60
11             MNSAGYEVFEVLS-------GQSFRCAEGQSVLRAMEA-QGKRCIPVG--CRGG-GCGLCRVRVLSG--- 56
24              MDKATLTFTDVS--------ITVNVPTGTRIIEMSEK-VGSGITYG---CREG-ECGTCMTHILEG-SE 55
Aae Fd1            MKVIINGKE----------FDIPKGVRFGELSHEIEKAGIEFG---CTDG-QCGVCVARVIKG-ME 51
                                                                  *     *  *

6          ----VDQSDQSFLDDD--QIEAG-YVLTCVAYPTS--DVVIQTHKEEDLY------------------------ 98
7          ----IDQSDQSFLDDD--QIEAG-YVLTCVAYPTS--DCTIKTHQEEGLY------------------------ 98
9          ----VDQSDQSFLDDD--QIEKG-FVLTCVAYPRS--DCKILTNQEEELY------------------------ 97
8          ----VDQSDQSFLDDD--QIEAG-YVLTCVAYPTS--DCTIETHKEEDLY------------------------ 96
4          ----VDQSDGSFLDDE--QMEQG-WVLTCVAFPTS--DVVIETHKEEELTA----------------------- 97
5          ----VDQSDGNYLDDD--QMADG-FVLTCVAYPQS--DVTIETHKEEELTG----------------------- 97
1          ----LNQDDQSFLDDD--QIDEG-WVLTCAAYPVS--DVTIETHKEEELTA----------------------- 96
2          ----IDQSDQSFLDDE--QMDAG-YVLTCHAYPTS--DVVIETHKEEEIV------------------------ 96
3          ----VDQSDQSFLNDN--QVADG-WVLTCAAYPTS--DVVIETHKEDDLL------------------------ 96
10         ----IDMDMQQILSDE--EVEDKNVRLTCIGSPDA--DEVKIVYNAKHLDYLQNRVI----------------- 128
14        KTGDKSAMEESMLDFA-ENVEPN-SRLSCQIKVSDALDGLVVRLPESQH------------------------- 105
15        EVGEPEAMEEDMLDFA-YDVQPN-SRLSCQIKVRDALDGLVVRVPERQG------------------------- 106
13        KLPKALPTETDMIDFA-YEPNPATSRLTCQIKVTSLLDGLVVHLPEKQI------------------------- 106
12        KVPAANEREIGMLECVTAELKPN-SRLCCQIIMTPELDGIVVDVPDRQW------------------------- 107
16        KLEAITDEENDMLDLA-YGLTDR-SRLGCQICLTKAMDNMTVRVPDAVSDARESIDMGMNSSKIE--------- 128
17        KLDAITDEENDMLDLA-YGLTDR-SRLGCQICLTKSMDNMTVRVPETVADARQSIDVGKTS------------- 124
18        ALPEPEDDENDMLDLA-YGLTET-SRLGCQIKMSKDIDGIRVALPQMTRNV-NNNDFS---------------- 172
19        KLKEAEEQEDDLLDMA-PFLREN-SRLGCQILLDKSMEGMELELPKAPGTS-TSMGTSQGHINIIVISRIINNI 95
23        SMEPSDELEDDMLDKA-WGLEPD-SRLSCQAVVAD--EDLVVEIPKYTINQVSEGH------------------ 112
22        SLEPSDELEDDMLDKA-WGLEPE-SRLSCQARVGT--EDLVVEIPRYTINQVSEQH------------------ 113
21        SLPESSEQEDDMLDKA-WGLEPE-SRLSCQARVTD--EDLVVEIPRYTINHAREH------------------- 111
20        SLSGWSEKEDDILDKA-WGLQSE-SRLSCQAVIGK--SDIEVEIPLYNLNYTVEY------------------- 111
11        ----AYRSGRMSRGHVPAKAAAEALALACQVFPQT--DLTIEYFRHVGGNKPDNMNYEEVTS------------ 112
24        NLSEPTALEMRVLEEN---LGGKDDRLACQCRVLG---GAVKVRPA---------------------------- 95
Aae Fd1   CLNEPSEEEEETLWRV--GAVDEDQRLTCQLVIEKE-DCDEIVIESED------------------------- 96
          ▲                          * *         ▲
```

FIGURE 1: Amino acid sequence alignment of plant- and mammalian-type [2Fe-2S] Fds. Sequences are designated by numbers as indicated hereafter. Genbank protein accessions are in parentheses. 1, *Spinacia oleracea* (spinach) FdI (FESP1); 2, *Petroselinum crispum* (parsley) Fd (A61291); 3, *Zea mays* (maize) Fd2 (T01170); 4, *Alocasia macrorrhizos* FdA (S28198); 5, *Datura stramonium* Fd (P81454); 6, *Anabaena* strain PCC7119 Fd (P06543); 7, *Spirulina platensis* Fd (FESGAL); 8, *Synechocystis* strain PCC6803 Fd (FEYB6); 9, *Synechococcus* sp. Fd (FEYCT); 10, *Haloarcula marismortui* (FEHSX); 11, *Pseudomonas putida* XylT (S16193); 12, *Pseudomonas putida* putidaredoxin (PXPSEP); 13, *Rhodobacter capsulatus* FdVI (S45612); 14, *Caulobacter crescentus* FdII (P37098); 15, *Mesorhizobium loti* Fd (BAB48308); 16, *Bos taurus* (bovine) adrenodoxin (BAA00363); 17, *Homo sapiens* (human) adrenodoxin (AXHU); 18, *Saccharomyces cerevisiae* Yah1p (S0006173); 19, *Drosophila melanogaster* Hsp-Fd (CAB55551); 20, *Buchnera* sp. APS Fd (BAB13290); 21, *Escherichia coli* Isc-Fd (P25528); 22, *Azotobacter vinelandii* Isc-Fd (FdIV) (T44286); 23, *Pseudomonas aeruginosa* PA01 Isc-Fd (NP_252498); 24, *R. capsulatus* FdIV (P16022); Aae Fd1, *Aquifex aeolicus* Fd1 (O67065). The full-length sequences of the mature proteins are shown, except in the cases of *H. marismortui* Fd (no. 10) and Yah1p (no. 18) where the 16 and 54, respectively, N-terminal residues have been omitted. The alignment has been done with CLUSTALW (*28*). Stars indicate totally conserved residues. Black triangles mark the two cysteine residues that are present in *A. aeolicus* Fd1 in addition to the four [2Fe-2S] cluster ligands.

and the $A_{420}/A_{280}$ absorbance ratio of the pure protein reaches 0.72 (Figure 3). Upon reduction to the $[2Fe\text{-}2S]^{+}$ level with dithionite, the absorbance decreases over the whole visible range, but a broad shoulder remains observable near 550 nm (Figure 3).

Resonance Raman spectroscopy in the Fe-S stretching region (250−450 $cm^{-1}$) is a sensitive structural probe for $S = 0$ $[2Fe\text{-}2S]^{2+}$ clusters and provides a means of distinguishing mammalian- and plant-type Fd $[2Fe\text{-}2S]^{2+}$ centers. Detailed vibrational assignments are available for representatives of both types of [2Fe-2S] Fd based on $^{34}S/^{32}S$ isotope shifts, studies of synthetic analogue complexes, and normal mode calculations (*34*−*37*). Figure 4 compares the resonance Raman spectra of oxidized *Aae* Fd1 with the human [2Fe-2S] Fd (Adx) and the plant-type *Anabaena* 7120 vegetative Fd, representative examples of mammalian- and plant-type [2Fe-2S] Fds, respectively. The resonance Raman spectra of *Aae* Fd1 and human Fd display closely similar band frequencies. They both differ significantly from the spectrum of plant-type (*Anabaena* 7120) Fd; i.e., frequency differences

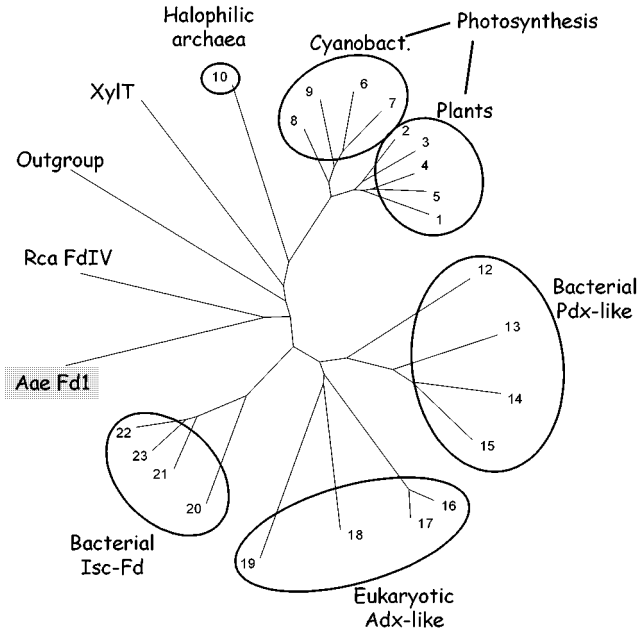


FIGURE 2: Graphical representation of the similarities between the sequences aligned in Figure 1. The dendrogram generated by CLUSTALW (*28*) was visualized using the TreeView (*29*) program. The outgroup sequences are those of three proteins from *Clostridium pasteurianum* that are unrelated to each other as well as to the Fds aligned in Figure 1 (Genbank protein entries in parentheses): rubredoxin (RUCLEP), 2[4Fe-4S] Fd (FECLCP), and [2Fe-2S] Fd (FECL2P). The sequence numbering code is as in Figure 1, except for *R. capsulatus* FdIV (no. 24 in Figure 1, here Rca FdIV), and XylT (no. 11 in Figure 1).

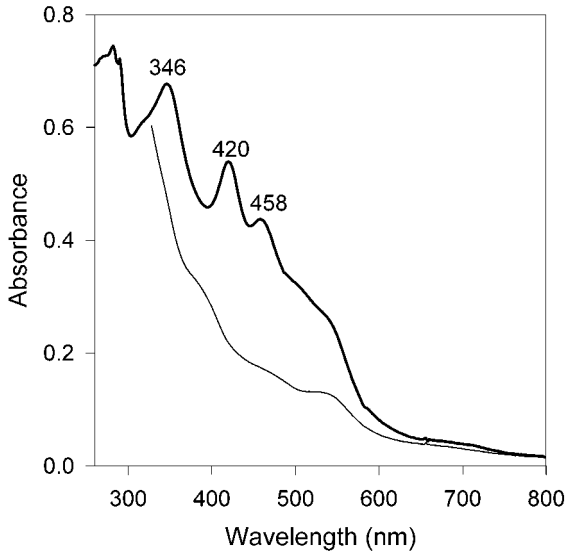


FIGURE 3: UV−visible absorption spectra of oxidized (thick line) and dithionite-reduced (thin line) Fd1 from *A. aeolicus*. The optical cell (path length: 1 mm) containing 0.25 mL of a 6 mg/mL solution of Fd1 (solvent: NaCl, 0.2 M, Tris-HCl, 20 mM, pH 8) was sealed with a rubber septum and flushed with argon. After the spectrum of the oxidized protein was recorded, 1 $\mu$L aliquots of a 20 mM dithionite solution were added until no further decrease of the absorbance occurred in the 400−500 nm region. The spectrum of the reduced protein was then recorded.

of up to 15 cm$^{-1}$ are observed for several bands (Figure 4, see also ref *36*). This indicates that the cluster environment of *Aae* Fd1, in the oxidized state, approximates that of a mammalian-type Fd. The resonance Raman spectrum of

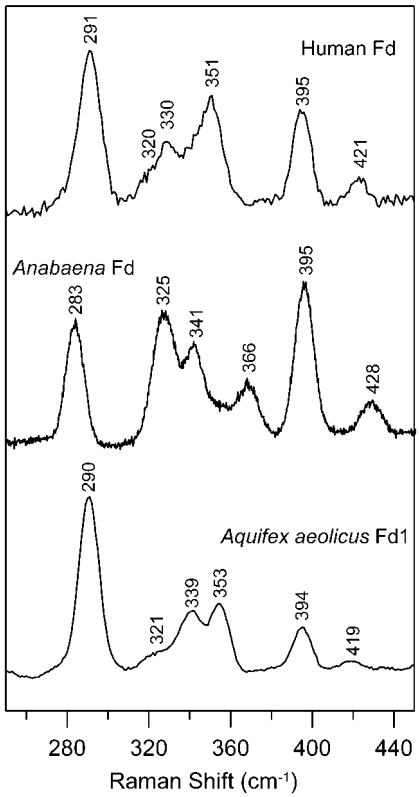


FIGURE 4: Comparison of the resonance Raman spectra of the [2Fe-2S]$^{2+}$ centers in human Fd, *Anabaena* 7120 vegetative Fd, and *A. aeolicus* Fd1. Spectra were recorded with 457.9 nm excitation using frozen droplets of concentrated samples (1−3 mM) maintained at 17 K. Bands originating from the frozen buffer solution have been subtracted from each spectrum.

oxidized *Aae* Fd1 was not perturbed by the addition of DTT (not shown), indicating that the [2Fe-2S]$^{2+}$ cluster environment is completely unaffected by the redox state of the disulfide (see below).

EPR and VTMCD spectroscopies provide complementary approaches for investigating the electronic properties of localized valence $S = {}^1/_2$ [2Fe-2S]$^+$ clusters. EPR provides a detailed assessment of the ground state *g*-value anisotropy that is determined primarily by distortions from idealized tetrahedral symmetry at the valence-localized ferrous site (*38*−*40*). In contrast, the VTMCD spectrum in the visible region is dominated by sulfur-to-ferric charge transfer transitions originating from the valence-localized ferric site (*37*, *41*). Moreover, both techniques have proven effective in distinguishing between mammalian and plant Fd-type [2Fe-2S]$^+$ centers (*37*, *41*). Comparisons of the EPR and VTMCD spectra of the [2Fe-2S]$^+$ centers in dithionite-reduced *Aae* Fd1, human [2Fe-2S] Fd, and *Anabaena* 7120 vegetative Fd are shown in Figures 5 and 6, respectively. The rhombic EPR spectrum of reduced *Aae* Fd1, $g = 2.05$, 1.96, 1.88, is analogous to the rhombic resonances observed in all plant-type Fds and is quite distinct from the axial EPR spectra, $g_{\|} \cong 2.02$ and $g_{\perp} \cong 1.95$, that are characteristic of the mammalian Adx-like, bacterial Pdx-like, and bacterial Isc Fds (*42*−*44*). The VTMCD spectrum of the [2Fe-2S]$^+$ center in *Aae* Fd1 is not closely similar to either one of the two reference spectra but nevertheless shares more characteristics (e.g., the 400 nm region and the absence of negative features near 600 nm) with plant-type (*Anabaena* 7120) Fd

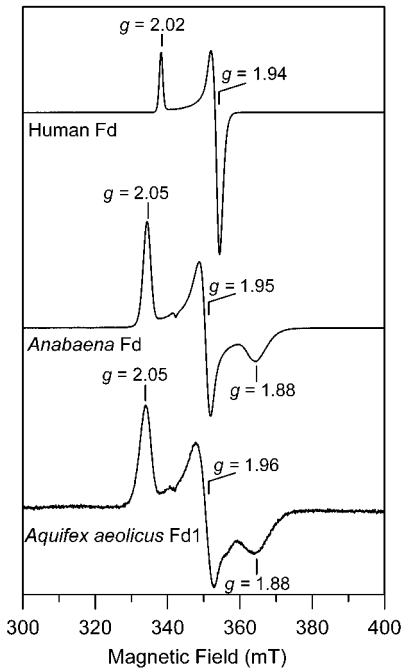


FIGURE 5: Comparison of the X-band EPR spectra of the $[2Fe\text{-}2S]^{+}$ centers in dithionite-reduced human Fd (adrenodoxin), *Anabaena* 7120 vegetative Fd, and *A. aeolicus* Fd1. The spectra were recorded at 20 K with a microwave power of 1 mW, modulation amplitude of 0.63 mT, and a microwave frequency of 9.0 GHz. The sample concentrations were in the range 0.25−0.5 mM, and all samples were 2 mM in sodium dithionite and contained 50% (v/v) ethylene glycol.

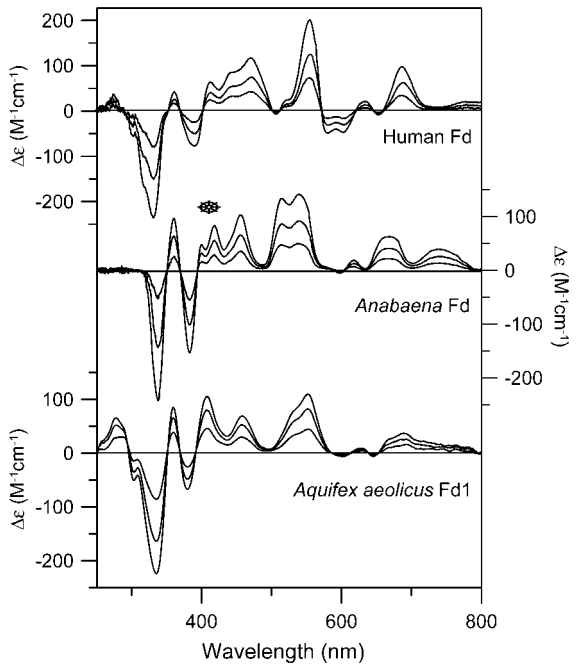


FIGURE 6: Comparison of the VTMCD spectra of the $[2Fe\text{-}2S]^{+}$ centers in dithionite-reduced human Fd (adrenodoxin), *Anabaena* 7120 vegetative Fd, and *A. aeolicus* Fd1. The spectra were recorded at 1.70, 4.22, and 10.25 K with an applied magnetic field of 6 T. All transitions increase in intensity with decreasing temperature. The samples are the same as those used for EPR studies and are described in the legend to Figure 5. The asterisk for *Anabaena* 7120 vegetative Fd indicates the center of a derivative feature from a minor heme impurity that is superimposed on a positive MCD band of the $[2Fe\text{-}2S]^{+}$ cluster.

spectra than with mammalian-type (human) Fd (Figure 6). Both the EPR and VTMCD spectra of dithionite-reduced *Aae* Fd1 were unaffected by the addition of DTT. However, the significance of this result is presently not clear because it is not known whether dithionite alone is able to reduce the disulfide in *Aae* Fd1 (see below).

Mössbauer spectra of oxidized and dithionite-reduced *Aae* Fd1 are shown in Figures 7 and 8, respectively. The zero-field spectrum of the oxidized protein (Figure 7A) consists of a quadrupole doublet with a line shape that suggests two distinct Fe sites. The solid line drawn through the data is a least-squares fit obtained by assuming the presence of two nested doublets, with $\Delta E_Q(1) = 0.76$ mm/s, $\delta(1) = 0.28$ mm/s and $\Delta E_Q(2) = 0.62$ mm/s, $\delta(2) = 0.26$ mm/s (0.27 mm/s line width at half-maximum). The four lines of the doublets can also be arranged in a nonnested fashion such that $\delta(1) = 0.23$ mm/s and $\delta(2) = 0.32$ mm/s. However, while such values could not readily be rejected for asymmetric coordination environments as those found in [2Fe-2S] clusters of the Rieske type, the tetrathiolate coordination expected here clearly favors the assignment that places the $\delta$ values near 0.27 mm/s. The 8.0 T spectrum (Figure 7 B) shows that both iron sites reside in a diamagnetic environment, in accord with observations reported for all clusters with $[2Fe\text{-}2S]^{2+}$ cores. The shape of the 8.0 T spectrum depends on the sign of $\Delta E_Q$ and the asymmetry parameter, $0 \leq \eta \leq 1$, of the electric field gradient (EFG) tensor. For the simulation of the spectrum of Figure 7B we have used $\Delta E_Q > 0$ and $\eta(1) = \eta(2) = 0.7$; however, combinations for which one $\eta$ value is larger than 0.7, with the other smaller than 0.7, are also possible.

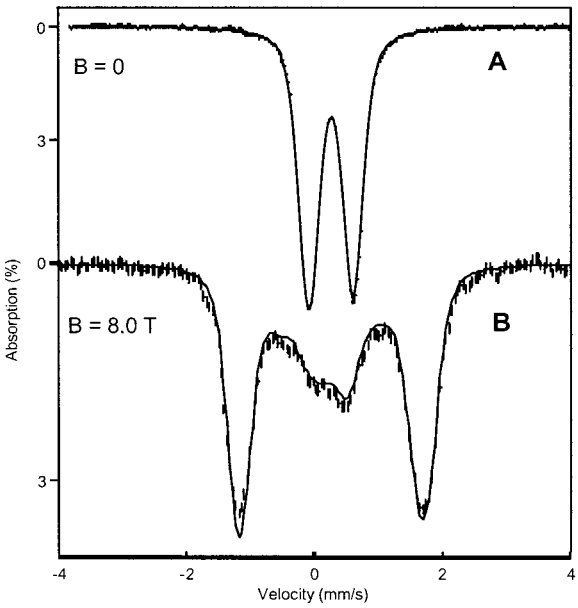


FIGURE 7: Mössbauer spectra of oxidized *A. aeolicus* Fd1 recorded at 4.2 K in zero field (A) and in a field of 8.0 T applied parallel to the observed $\gamma$-radiation (B). The solid lines are spectral simulations for two sites using the parameters quoted in the text.

Figure 8 shows 4.2 K spectra of dithionite-reduced *Aae* Fd1 recorded in external magnetic fields as indicated. The spectral patterns observed are very similar to those reported for other $[2Fe\text{-}2S]^{1+}$ clusters. The analysis of such spectra has been described in considerable detail elsewhere (*45*, *46*).

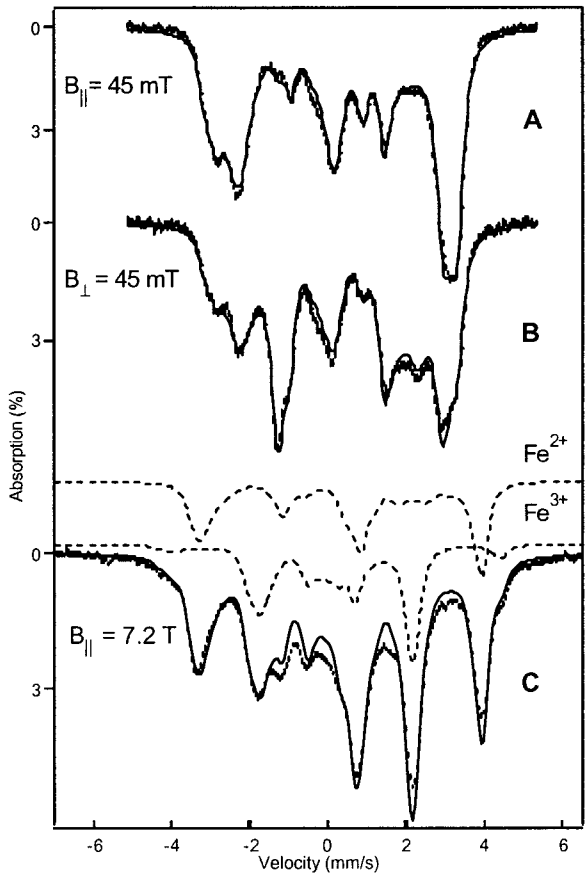


FIGURE 8: Mössbauer spectra of reduced *A. aeolicus* Fd1 recorded at 4.2 K in applied magnetic fields. (A) 0.045 T parallel, (B) 0.045 T transverse, and (C) 7.2 T parallel to the observed $\gamma$-radiation. The solid lines drawn through the spectra are spectral simulations based on eq 1 using the parameters listed in Table 1. The contributions of the ferric and ferrous sites are shown separately (dashed lines) above the 7.2 T data.

The spectra of Figure 8 were simulated with the $S = {}^1/_2$ spin Hamiltonian

$$H = \beta \mathbf{S}\cdot\mathbf{g}\cdot\mathbf{H} + \sum_{i=1}^{2}\left\{\mathbf{S}\cdot\mathbf{A}(i)\cdot\mathbf{I}(i) - g_n\beta_n\mathbf{B}\cdot\mathbf{I}(i) + \frac{eQV_{\zeta\zeta}(i)}{12}[3\mathbf{I}_\zeta{}^2 - {}^{15}/_4 + \eta(i)(\mathbf{I}_\xi{}^2(i) - \mathbf{I}_\eta{}^2(i))]\right\} \quad (1)$$

where all quantities have their conventional meanings and where $S$ is the system spin of the exchange-coupled cluster. $(\xi,\eta,\zeta)$ designates the principal axis system of the EFG-tensor. A spectrum recorded at 190 K exhibited broad and unresolved features characteristic of intermediate relaxation of the electronic spin, preventing us from determining $\Delta E_Q$ and $\delta$ of the two Fe sites independently at high temperature. Thus, all unknowns (12) had to be determined from the low-temperature spectra. For the analysis the spectrum of Figure 8C (7.2 T applied field) was most informative as the contributions of the ferric and ferrous site are best resolved in a strong applied field (simulated spectra of the $Fe^{2+}$ and $Fe^{3+}$ sites are shown separately above the experimental data). For proper simulations of the features of the ferrous sites, the largest component of the (axial) EFG-tensor has to be positive and directed along the smallest component of the *A*-tensor. The solid lines drawn through the experimental data are spectral simulations based on eq 1 using the parameters listed in Table 1. Overall, the simulations represent the data quite well. However, there are some broader features (representing less than 10% of the total Fe) in the central part of the 7.2 T spectrum which have not yet been assigned.

*Redox Potential*. The redox potential of *Aae* Fd1 has been measured by reductive (with dithionite) and oxidative (with ferricyanide) spectrophotometric titration (Materials and Methods). The data from a typical titration are shown in Figure 9. The measured redox potential of $-375 \pm 5$ mV is in the upper range of the potentials reported for plant-type Fds and significantly more negative than those of Adx-like proteins (*6*).

*Disulfide Bridge in Aae Fd1*. The sequence of *Aae* Fd1 includes two cysteine residues in addition to the four required as ligands of the [2Fe-2S] cluster (Figure 1). This raised the possibility that a disulfide bridge may exist in *Aae* Fd1, as in a few other Fds (*52*−*56*). The first hint was the observation that the half-life of Fd1 at 100 °C was decreased ca. 20-fold (180−10 min) in the presence of a disulfide reducing agent (DTT). In contrast, DTT had no effect on the thermal stability of *A. aeolicus* Fd4 (J. Meyer, unpublished observations), another hyperthermophilic [2Fe-2S] Fd having only four cysteine residues (*3*, *27*). The question was then addressed by preparing the C87A variant of *Aae* Fd1, in which the putative disulfide bond cannot exist. Preliminary experiments showed that the thermal stability of C87A Fd1, as compared to WT Fd1, is lowered to a similar level as that of WT Fd1 in the presence of DTT. A more detailed comparative analysis of the stability of WT and C87A is described below.

Further evidence supporting the existence of a disulfide bond in *Aae* Fd1 was sought by implementing thiol reagents. In one set of experiments the proteins were labeled with a fluorescent alkylating agent and analyzed by SDS−PAGE, and the gels were inspected under UV illumination prior to protein staining (Materials and Methods, (*20*)). The data reveal (Figure 10) that the C87A variant is rapidly alkylated, while labeling of WT Fd1 only occurs after preincubation with DTT. In another series of experiments, the reactivity of Fd1 with 5,5′-dithiobis(2-nitrobenzoic acid) (DTNB) was monitored spectrophotometrically by measuring the absorption increase at 412 nm resulting from the buildup of TNB (Figure 11). DTNB did not react with WT Fd1 whereas C87A caused a rapid release of TNB produced by the reaction of DTNB with free thiol(s). The absorption increase corresponded to the reaction of 1.05 free −SH groups per protein molecule. This value, together with the absence of absorption changes in the region (550−600 nm) where the absorbance of DTNB and TNB is negligible, indicated that the [2Fe-2S] chromophore is unaffected by the reaction.

These data are consistent and strong indications that a disulfide bridge is present in *Aae* Fd1. This disulfide bridge appears to have no bearing on the properties of the $[2Fe\text{-}2S]^{2+}$ chromophore since removal of this disulfide link in C87A Fd1 does not cause any modification of the UV−visible absorption spectrum (Figure 11). Likewise, reduction of the disulfide bond causes no change in the RR spectrum (see above). The redox potential of the metal site is also unaltered by the C87A mutation (Figure 9), but it is then likely that the disulfide bond of WT Fd1 is reduced and broken in the redox potential range (below −300 mV) where

Table 1: Mössbauer and EPR Parameters of Selected $[2Fe\text{-}2S]^{+}$ Proteins

| | $Fe^{3+}$ | | | | | | $Fe^{2+}$ | | | | | | |
|---|---|---|---|---|---|---|---|---|---|---|---|---|---|
| protein[a] | $\Delta E_Q$ (mm/s) | $\eta$ | $A_x$ (MHz) | $A_y$ (MHz) | $A_z$ (MHz) | $\delta$ (mm/s) | $\Delta E_Q$ (mm/s) | $\eta$ | $A_x$ (MHz) | $A_y$ (MHz) | $A_z$ (MHz) | $\delta$ (mm/s) | $g_x, g_y, g_z$ |
| spinach | 0.64 | −0.6 | −51 | −49.1 | −42 | 0.29[b] | −3.0 | 0 | 11.1 | 16.8 | 35.3 | 0.63[b] | 1.90, 1.96, 2.05[c] |
| parsley | 0.68 | −0.9 | −51 | −46.2 | −42 | 0.29[b] | −3.0 | 0 | 11.2 | 14.0 | 33.6 | 0.63[b] | 1.89, 1.96, 2.05[c] |
| *S. lividus* | 0.6 | −0.3 | −51.6 | −50.0 | −42.0 | 0.29[b] | −3.20 | 0 | 13.0 | 15.0 | 36.5 | 0.63[b] | 1.89, 1.96, 2.05[c] |
| *P. putida* | 0.6 | 0.5 | −56.5 | −50.5 | −43.3 | 0.35 | 2.7[d] | 0 | 14.1 | 21.3 | 35.4 | 0.65 | 1.94, 1.94, 2.01[c] |
| ferrochelatase | 1.2 | 0 | −56.2 | −46.0 | −43.2 | 0.28 | 3.3[d] | 0 | 11.0 | 29.5 | 29.5 | 0.67 | 1.91, 1.93, 2.00 |
| 2Fe*Cp*Fd | 1 | 0.3[e] | −57.0 | −49.0 | −41.0 | 0.34 | 3.2[d] | 0.2 | 9.7 | 28 | 32 | 0.65 | 1.92, 1.95, 2.00 |
| *Aae* Fd1 | 1.0(2)[f] | 0 | −56(2) | −49(2) | −42(3) | 0.30(4) | 3.0(2)[d] | 0 | 11(1) | 27(2) | 33(4) | 0.62(2) | 1.88, 1.96, 2.05 |

[a] The [2Fe-2S] proteins listed here are the plant-type Fds from spinach (*Spinacia oleracea*), parsley (*Petroselinum crispum*) (*47*), and the blue-green alga *Synechococcus lividus* (*48*); putidaredoxin from *Pseudomonas putida* (*46*); mouse (*Mus musculus*) ferrochelatase (*49*); *Clostridium pasteurianum* [2Fe-2S] ferredoxin (*17*, *50*); *A. aeolicus* Fd1 (this work). [b] The isomer shifts given in refs *47* and *48* were relative to $^{57}Co$ diffused into platinum. The corrections needed to relate these shifts to Fe metal at 298 K (used in this work) give rise to some inconsistencies. We have therefore used the values vs Fe metal, after correcting for second-order Doppler shifts, which were reported in another study of spinach Fd (*51*), although these authors have not determined the *A*-tensors. Since it was reported that spinach, parsley, and *S. lividus* Fds have the same $\delta$-values (*47*, *48*), we have entered the $\delta$-values of ref *51* for all three plant-type Fds. [c] For spinach, parsley, and *S. lividus* Fds, as well as for putidaredoxin, the spatial correlations between the *A*-tensors and the *g*-tensors have been established by ENDOR (*47*, *48*). Such data are not available for ferrochelatase, 2Fe*Cp*Fd, and *Aae* Fd1. [d] Following conventional usage we have quoted the EFG-tensors in their principal axis systems ($\xi,\eta,\zeta$). For plant-type Fds these systems coincide with ($x,y,z$) of the *A*- and *g*-tensors; for the other proteins the symmetry axis of the EFG-tensor, $\zeta$, is along the *x*-axis of the *A*-tensor frames. [e] Table 2 of ref *50* has a typographical error for the ferric site; $\eta = -2.0$ should be replaced by $\eta = +2.0$. In a proper coordinate system for which $0 \leq \eta \leq 1$, this new value translates to $\Delta E_Q = +1.0$ mm/s and $\eta = 0.3$. [f] Numbers in parentheses give estimated uncertainties in the last relevant digit.

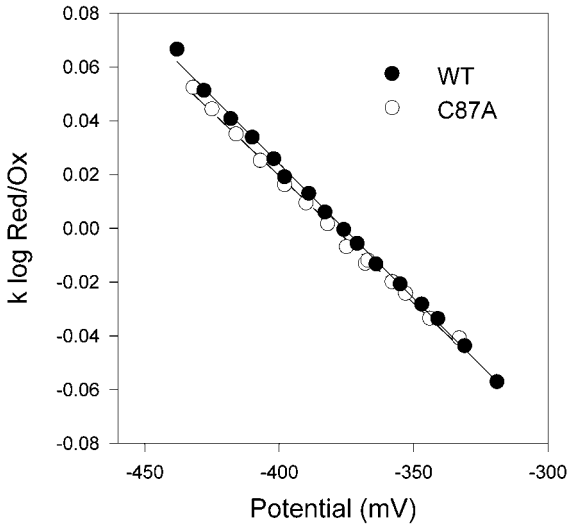


FIGURE 9: Redox titrations of *A. aeolicus* Fd1. Measurements were carried out as described in Materials and Methods. Data shown are from oxidative titrations (with ferricyanide) of dithionite-reduced WT (closed circles and solid line) and C87A (open circles and dashed line) *A. aeolicus* Fd1. The redox potential values obtained by linear regression (lines) on the data points were −375 and −380 mV for WT and C87A, respectively. The averages of several (four for WT, two for C87A) reductive and oxidative titrations were 375 ± 5 mV for both proteins.

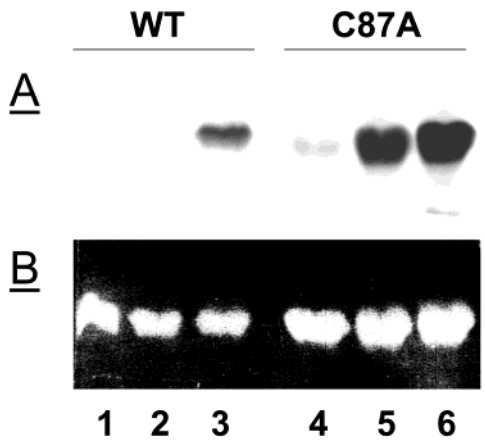


FIGURE 10: Reactivity of *A. aeolicus* Fd1 with the fluorescent thiol reagent I-AEDANS. Reactions were as in Materials and Methods. The SDS−PAGE gel (5% stacking, 20% analysis) was visualized under UV illumination (A) and subsequently stained for protein (B). Lanes 1−3: WT Fd1. Lanes 4−6: C87A Fd1. Lanes 1 and 4: controls with DTT added before I-AEDANS. Lanes 2 and 5: normal alkylation reactions. Lanes 3 and 6: alkylation after preincubation (30 min) of the proteins (50 $\mu$M) in the presence of 0.5 mM DTT.

the measurements are made. While the disulfide bond does not appear to have any bearing on the properties of the [2Fe-2S] cluster, it does contribute considerably to the stability of the protein, as shown in more detail in the next section.

*Chemically Induced Unfolding of Fd1.* The chemical denaturant GuHCl was used to promote unfolding of WT and C87A Fd1 at various pH values at 20 °C. The native state of Fd1 is characterized by negative CD intensity around 210−220 nm due to secondary structure, a quenched tryptophan emission due to energy transfer to the Fe-S center (centered around 355 nm), and distinct visible absorption between 350 and 500 nm arising from the $[2Fe\text{-}2S]^{2+}$ cluster. Upon Fd1 unfolding, the far-UV CD signal disappears, the tryptophan emission increases, and the visible absorption diminishes (Figure 12). Therefore, Fd1 unfolding was monitored by far-UV CD, fluorescence, and visible absorption.

GuHCl-induced Fd1 unfolding is irreversible, as concluded from dilution tests of unfolded samples to conditions favoring the native state. This means that true equilibrium is never established in the titration experiments (*57*); therefore, we only describe the unfolding data in terms of transition midpoints for various incubation times (Table 2). Most likely, the lack of refolding is due to Fe-S cluster decomposition in the denatured state. This is in accord with the disappearance of visible absorption upon Fd1 unfolding (Figure 12C) and agrees with reports on other Fds (*58*, *59*). At all conditions studied, with both WT and C87A Fd1, we observe single, cooperative unfolding transitions. Moreover, the kinetic traces collected upon triggering unfolding are identical regardless

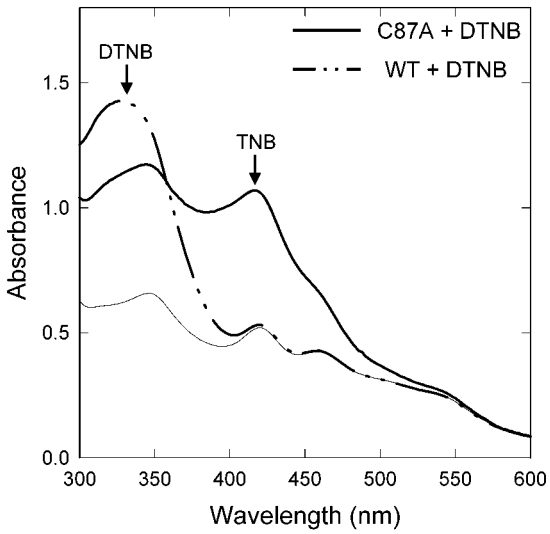


FIGURE 11: Reactivity of *A. aeolicus* Fd1 with DTNB. DTNB (50 $\mu$M final concentration) was added to protein solutions (50 $\mu$M) in Tris-HCl, 50 mM, pH 8.0. Spectra shown are as follows: WT or C87A Fd1 prior to the addition of DTNB (thin line); C87A Fd1 20 min after the addition of DTNB (thick solid line); WT Fd1 20 min after the addition of DTNB (thick dashed line). The half-time of the reaction of DTNB with C87A Fd1 was ca. 2 min. Absorption maxima of DTNB and TNB near 340 and 420 nm, respectively, are indicated by arrows.

of whether far-UV CD, fluorescence, or visible absorption is used as the detection probe (data not shown). These findings suggest that there are no detectable intermediates on the Fd1 unfolding pathway.

At pH 7 (20 °C), WT Fd1 is highly resistant toward chemical perturbation. Very high concentrations of GuHCl and long incubation times are required to promote unfolding. For example, there is no unfolding at all observed at pH 7 in the presence of 7.9 M GuHCl (the highest possible concentration) within the first 2 h; the observed transition midpoints are 7.2 and 6.5 M GuHCl after 12 and 24 h of incubation, respectively (Table 2). At pH 10, Fd1 is barely less stable than at pH 7, while at pH 2.5 the stability undergoes a significant decrease: the transition midpoint after 12 h of incubation is lowered from 7 to 7.2 (pH 7 and 10) to 5.0−5.4 (Table 2). The transition midpoints determined by the different spectroscopic probes at identical incubation times roughly agree with each other (Table 2), suggesting again that Fd1 unfolding is an apparent two-state process without populated intermediates.

The C87A variant of Fd1 shows lower stability toward chemical denaturation than WT Fd1 (Table 2). For 12 h of incubation, at pH 7, the transition midpoints are 6.2 and 7.2 M GuHCl for C87A and WT Fd1, respectively. At pH 2.5 they are 4.6 and 5.4 M GuHCl for C87A and WT Fd1, respectively. These findings support the hypothesis that cysteine 87 forms a disulfide bridge in WT Fd1 and that this bond stabilizes the native structure of Fd1.

Table 2: Transition Midpoints ($[GuHCl]_{1/2}$) for GuHCl-Induced Unfolding (20 °C) of WT and C87A Fd1 Proteins in Various Solution Conditions, at Various Incubation Times, As Measured by Different Spectroscopic Techniques[a]

| solution condition | probing technique | incubation time (h) | $[GuHCl]_{1/2}$ (M) | |
|---|---|---|---|---|
| | | | WT Fd1 | C87A Fd1 |
| pH 7 | $abs_{418nm}$ | 2 | no unfolding | 6.5 |
| | | 12 | 7.2 | |
| | | 24 | 6.7 | 6.1 |
| | $em_{365nm}$ | 24 | 6.4 | 6.2 |
| | $CD_{220nm}$ | 2 | | 6.8 |
| | | 12 | 7.2 | 6.2 |
| | | 24 | 6.4 | |
| pH 2.5 | $abs_{418nm}$ | 1 | 6.6 | 6.2 |
| | | 12 | 5.4 | 4.6 |
| | $em_{365nm}$ | 1 | 6.5 | 6.7 |
| | | 12 | 5.3 | 4.8 |
| | $CD_{220nm}$ | 12 | 5.0 | 4.4 |
| pH 10 | $abs_{418nm}$ | 1 | 7.5 | 5.2 |
| | | 12 | 7.1 | 5.1 |
| | $em_{365nm}$ | 12 | 7.0 | 5.1 |
| | $CD_{220nm}$ | 12 | 7.0 | 5.3 |

[a] Absorption decrease at 418 nm, emission increase at 365 nm, and far-UV CD decrease at 220 nm.

*Thermally Induced Unfolding of Fd1*. Thermal unfolding of Fd1 is also irreversible: cooling of heated samples does not restore spectroscopic features characteristic of the native protein. Since the irreversibility is most likely due to degradation of the Fe-S cluster in the unfolded state, we assumed the following mechanism [equilibrium established rapidly for the first reaction, while the irreversible second step is slower (*60*)]:

$$\text{folded} \leftrightarrow \text{unfolded} \rightarrow \text{denatured}_{irr}$$

It is then possible to eliminate the influence of the irreversible step by extrapolating values for thermal midpoints ($T_m$) at various scan rates to infinite scan rate (*60*). The thermal experiments were monitored by visible absorption and performed at three different scan rates in the presence of various GuHCl concentrations. First, $T_m$ values at various GuHCl concentrations were extrapolated to yield $T_m$ in 0 M GuHCl for each scan rate (Figure 13). These $T_m$ values were

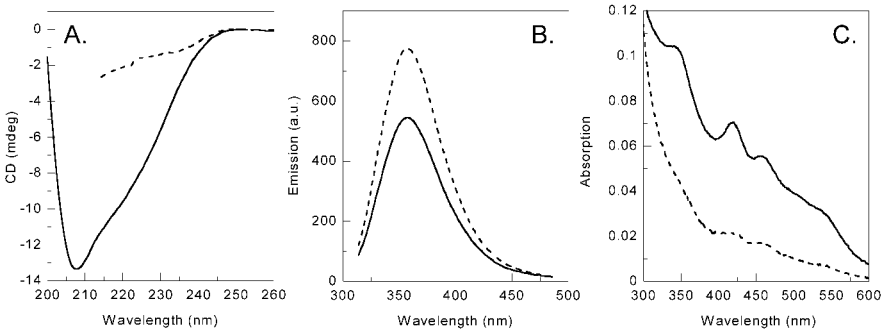


FIGURE 12: Folded (solid line) and unfolded (dashed line) states of Fd1 (pH 7, 20 °C) as probed by (A) far-UV CD, (B) tryptophan emission (excitation 280 nm), and (C) visible absorption.

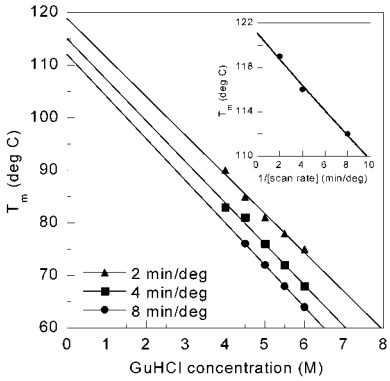


FIGURE 13: Thermal midpoints ($T_m$) versus GuHCl concentrations present in the Fd1 samples obtained at three different scan rates (2, 4, and 8 min/deg). A linear least-squares fit of the values for each scan rate provided, by extrapolation, $T_m$ in the absence of denaturant (pH 7). Inset: $T_m$ in the absence of denaturant (pH 7) as a function of 1/(scan rate). Extrapolation to 0 on the *x*-axis yielded the $T_m$ value at infinite scan rate (Table 3).

Table 3: Thermal Midpoints ($T_m$), Extrapolated to Infinite Scan Rate To Eliminate the Irreversible Step (*60*), for WT and C87A Fd1 Proteins

| | $T_m$ (°C) | |
|---|---|---|
| solution condition | WT Fd1 | C87A Fd1 |
| pH 2.5 | 79 | 68 |
| pH 7 | 121 | 113 |
| pH 10 | 116 | |

then extrapolated to infinite scan rate, which yielded a value of 121 °C (inset, Figure 13; Table 3). The data shown in Figure 13 were collected at pH 7. Similar sets of data were obtained at pH 2.5 and 10 (Table 3). Thermal unfolding shows a pH dependence trend similar to that found in the chemical denaturant studies, pH 2.5 being significantly more destabilizing than pH 10.

In keeping with its lower stability toward chemical perturbation, C87A Fd1 is also less stable than WT Fd1 toward thermal unfolding. $T_m$ for C87A unfolding at pH 7 (0 M GuHCl; infinite scan rate) is 113 °C, i.e., 8° lower than the $T_m$ for WT Fd1 (Table 3). This is consistent with the much higher rate of thermal denaturation under isothermal incubation at 100 °C of C87A ($t_{1/2}$ = 10 min) as compared to WT Fd1 ($t_{1/2}$ = 180 min; see above).

## DISCUSSION

The gene encoding Fd1 (orf 919a) is located ca. 50 bp downstream of the *ftsY* gene in the *A. aeolicus* genome (*13*) and is apparently monocistronic. While the work reported here shows that *fd1* encodes a stable [2Fe-2S] Fd, the expression of that gene in *A. aeolicus* and the function of its product remain open questions. *Aae* Fd1 has a primary structure that clearly relates it to the plant- and mammalian-type [2Fe-2S] Fds. Alignments of a representative sample of sequences (Figures 1 and 2) nevertheless revealed that *Aae* Fd1 does not belong to any of the main subgroups of this class of Fds. Indeed, the dendrogram shows that it maps, together with a few other proteins, in a region located between the plant- and adrenodoxin-type Fds. These atypical Fds are not closely clustered in the dendrogram and have uncommon (*30*) and sometimes not fully elucidated (*31, 32*) functions. It is therefore difficult to derive from these similarities useful indications regarding the function of *Aae* Fd1. It is nevertheless worth noting that the closest relatives of *Aae* Fd1 appear to be the Isc-Fds found in many bacteria (*7*−*9*, *61*). Unlike the latter, however, the *Aae* Fd1-encoding gene is not part of an *isc* operon. In fact, while *nif*S-, *nifU*-, and *iscA*-like genes are present in the genome of *A. aeolicus*, they are scattered, and none of them occurs near to *fd1* (*13*).

The amino acid sequence and composition of *Aae* Fd1 display peculiarities that are worth considering in relation with the exceptional thermostability of this protein. One striking feature is the high proportion of charged residues (over 36%) which largely exceeds that of its mesophilic counterparts, e.g., plant Fds (ca. 25%) (Figure 1). All of these proteins are very acidic (p$I$ = 4.2), and the additional charged residues present in *Aae* Fd1 are evenly distributed between acidic (mostly glutamates) and basic (mostly lysines) ones. Such variations in amino acid composition have been observed in comparisons of large numbers of mesophilic and hyperthermophilic proteins (*62*). A relatively high density of surface charges is observed in many hyperthermophilic proteins and is believed to contribute significantly to protein stability by increasing the number of salt bridges (*62*−*66*). A notable deviation from this trend appears to occur among the 2[4Fe/3Fe-4S] Fds, where hyperthermophiles surprisingly display a relative increase in the proportion of hydrophobic, rather than charged, surface residues (*67*).

The metal site of *Aae* Fd1 displays the spectroscopic characteristics of [2Fe-2S] clusters with all-cysteine ligation. However, even within this framework there are variations, and subfamilies are thereby readily identified (*37*). The UV−visible and resonance Raman spectra indicate that the oxidized $[2Fe\text{-}2S]^{2+}$ level of *Aae* Fd1 is most similar to that of the Fds involved in hydroxylation/oxygenation reactions. As to the $[2Fe\text{-}2S]^{+}$ reduced level, the EPR *g*-values listed in Table 1 (see also Figure 5) would seem to suggest that the ferrous site is similar to that of plant-type ferredoxins. However, the $^{57}$Fe hyperfine parameters contradict such a conclusion. Indeed, comparison of the ferrous site parameters listed in Table 1 reveals two groups of Fds which differ in two ways. The first group comprises the plant-type Fds and the second one the other proteins listed in the table. The ferrous sites of the two groups display two distinct differences: namely, (i) while all *A*-tensors, with the exception of putidaredoxin, are roughly axial, those of the plant-type Fds exhibit one large and two small components while those of the second group have two large and one small component; (ii) the electric field gradient (EFG) tensors of all ferrous sites are axial ($\eta \approx 0$), or nearly so, but those of plant-type Fds exhibit a negative $\Delta E_Q$ while the other proteins have a positive $\Delta E_Q$. (The sign of $\Delta E_Q$ reflects the sign of the largest component of the EFG-tensor. $\Delta E_Q < 0$ and $\eta = 0$ indicates a $d_{z^2}$ ground state.) The correlations between properties i and ii are well understood (*39*). These observations suggest that the ferrous site of reduced *Aae* Fd1 differs from those of plant-type ferredoxins but is quite similar to those of mammalian ferrochelatase and [2Fe-2S] *Cp*Fd and somewhat similar to that of putidaredoxin. However, we note that the *g*-values, and particularly the largest one, of *Aae* Fd1 differ from those of the latter proteins. This discrepancy suggests that some of the observed similarities between the ferrous sites of ferrochelatase, [2Fe-2S] *Cp*Fd, and *Aae* Fd1 may be coincidental. Indeed, the

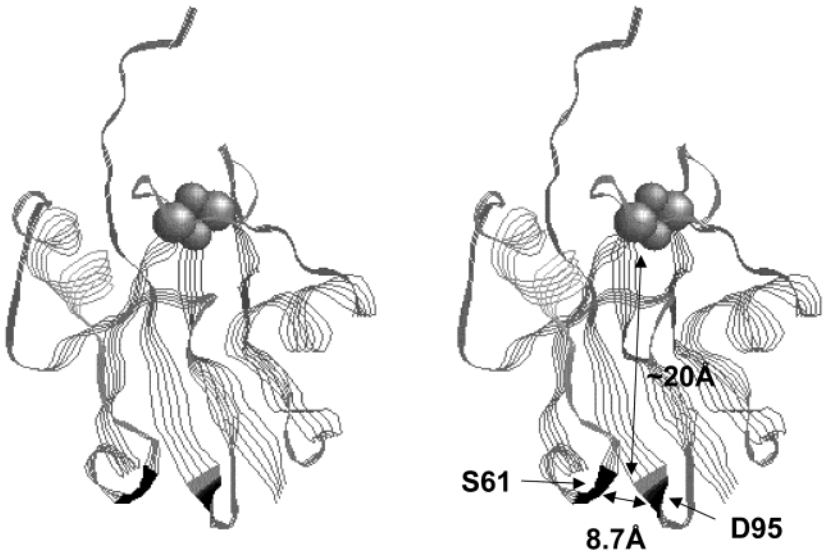


FIGURE 14: Stereoview of the *E. coli* [2Fe-2S] Fd structure (*61*; PDB entry 1I7H). The iron (smaller spheres) and sulfide (larger spheres) atoms of the [2Fe-2S] site are shown in CPK. The main chain parts of Ser61 and Asp95 are shown in black (arrows). These residues are the counterparts (see Figure 1) of the two cysteine residues (Cys52 and Cys87) that form the disulfide bond in *A. aeolicus* Fd1. The figure shows that this disulfide bond straps two neighboring parallel loops, with the reasonable assumption that the two proteins assume similar folds. The distance (8.7 Å) between the Cα atoms of the indicated residues is longer than in known cystine units (ca. 5.5 Å) but might be shortened by small displacements of the loops. Also shown is the distance (ca. 20 Å) between the putative disulfide bond and the [2Fe-2S] cluster. This distance is twice as long as the one separating the disulfide bond and the [4Fe-4S] cluster in *T. maritima* Fd (*67*). The structure was drawn using RASMOL (*72*).

polypeptide folds around the metal sites of these three proteins are quite different (*3*, *68*; this work), and in addition the orientation of the *g*-tensor relative to the *A*- and EFG-tensors is unknown for all of them. That some of these similarities may be coincidental is also indicated in the Bertrand and Gayda (*39*) model: for instance, two sets of crystal field parameters ($\theta = 30°$ and $\theta = -30°$) produce collinear axial *A*- and EFG-tensors with $\Delta E_Q > 0$, and a third solution arises for a ground state having $d_{xy}$ symmetry (*x* and *y* refer to the coordinate system of ref *39*). The unique axes of these three tensors are along *x*, *y*, or *z*, respectively. We note that $A_x(Fe^{3+})$ of *Aae* Fd1 compares well with ferrochelatase, *Cp*Fd, and putidaredoxin but differs significantly from the $A_x$ values of the plant-type Fds (Table 1). Moreover, *Aae* Fd1 shares with the latter proteins remarkably long relaxation times of the electronic spin at high temperatures (e.g., 200 K). Finally, we note that the four spectroscopic techniques employed here explore different aspects of the cluster's electronic structure. The resonance Raman spectra probe the diferric state of the cluster. In the mixed-valence state, the MCD spectra are most sensitive to the ferric site while EPR probes essentially the ferrous site; in contrast, the Mössbauer spectra probe quite sensitively the electronic structure of both sites. Clearly, further studies are required to delineate the similarities and dissimilarities of the clusters discussed here.

Altogether, the spectroscopic data suggest that the $[2Fe\text{-}2S]^{2+/+}$ site of *Aae* Fd1 differs from its counterparts in both the plant-type and the mammalian-type Fds. It nevertheless seems to be more closely related to the latter than to the former. A more detailed interpretation would require additional spectroscopic data, as well as data that would complement the high-resolution structures of both redox levels of plant-type Fds (*69*), namely, the collection of a similar set of data on other subgroups of the plant- and mammalian-type Fds.

While the properties of its [2Fe-2S] active site are not unusual, *Aae* Fd1 has one distictinctive feature, namely, a cystine unit, that is of rather uncommon occurrence among Fds. The published data include a crystal structure (*52*), NMR, Mössbauer and redox titrations (*53*) for *Desulfovibrio gigas* [3Fe-4S] FdII, a crystal structure for *Thermotoga maritima* [4Fe-4S] Fd (*56*), NMR, redox cycling, and chemical modification for *Pyrococcus furiosus* [3Fe-4S]/[4Fe-4S] Fd (*54*, *70*), and NMR for *Thermococcus litoralis* [4Fe-4S] Fd (*71*) and *Synechocystis* PCC6803 [2Fe-2S] Fd (*55*). In the latter case the authors regarded their data as merely suggestive of the existence of a disulfide bond. They also pointed out that, on the basis of X-ray structures of homologous proteins, the two residues might be too far apart to form a disulfide bridge. Thus, the data presented here on *Aae* Fd1 would appear to constitute the first strong evidence for the presence of a cystine unit in a [2Fe-2S] Fd. In the absence of structural data for *Aae* Fd1, crystal structures of homologous proteins have been inspected to assess the localization and likelihood of this disulfide bond. Among the proteins of known structure, *E. coli* Fd (*61*) is the closest relative of *Aae* Fd1 (Figures 1 and 2). It has therefore been used as a model for the localization of the cysteine residues involved in the disulfide bond of *Aae* Fd1 (Figure 14). It appears that this disulfide bond would strap two adjacent loops of the protein, which makes sense with respect to its stabilizing effect on the structure. The distance between the Cα atoms of the relevant residues in the *E. coli* Fd structure (*61*) exceeds the one occurring in cystine units (8.7 vs 5.5 Å) but could easily be decreased in *Aae* Fd1 by a slight shift of the loops involved. It is also noted that the distance between the Fe-S cluster and the disulfide bond (ca. 20 Å) is much larger than in *T. maritima* Fd [ca. 10 Å (*56*)].

The presence of a disulfide bond in *Aae* Fd1 must have bearings on the redox activity of the protein. In this respect, *P. furiosus* Fd is the best studied example: the four states

resulting from the coexistence of two redox-active sites ([4Fe-4S] cluster and disulfide bridge) have been evidenced and studied in detail (*54*, *70*). The disulfide bond of *P. furiosus* Fd has been shown to exist in two isomeric forms, the less stable of which predominates at high temperatures (*70*). This makes the disulfide bond more easily reducible in the temperature range where the host organism thrives and suggests that the thiol/disulfide redox couple might have a physiological role. Whether *Aae* Fd1 displays a similar behavior remains an open question. A key point in this respect is the yet unknown redox potential of the dithiol/disulfide couple. These matters will be addressed in a separate investigation implementing NMR techniques along with biochemical approaches (J. Meyer and J. Gaillard, work in progress).

The most prominent role of the disulfide bond in *Aae* Fd1 is the stabilization of the protein. This effect has been clearly demonstrated here and is a rather novel occurrence among Fds. While the characterized hyperthermophilic [4Fe-4S] Fds do have a disulfide bond in the region of the missing second [4Fe-4S] cluster (*54*, *56*, *70*, *71*), no data have been brought forth that might suggest a role of that bond in the thermostability of these proteins (*73*). On the contrary, the predominance of the less stable conformation of the disulfide bond at high temperature in *P. furiosus* Fd (*70*) suggests that it has no stabilizing effect. It is also recalled that at least one mesophilic member of this protein family does possess a similarly positioned cystine unit (*52*). In plant-type Fds likewise, the putative disulfide bonds have not been reported to increase protein stability. Besides, these bonds appear to be present not only in thermophilic organisms (*55*, *74*). Thus, *Aae* Fd1 would be the only demonstrated case of Fd stabilization by a disulfide bond. It is also the only hyperthermophilic [2Fe-2S] plant-type Fd characterized so far. It therefore remains to be established whether, for these proteins, the presence of a disulfide bond is a requirement for hyperthermostability or just an idiosyncrasy of *Aae* Fd1. An answer to this question will be sought through the investigation of another plant-type Fd from *A. aeolicus* which lacks the supplementary cysteine residues required for the formation of a disulfide bond (J. Meyer, unpublished observations).

The redox activity of the disulfide bond of *Aae* Fd1, together with its enhancing effect on the thermostability of the protein, may be an important issue with respect to the stability of the protein in vivo. Indeed, since the disulfide form ($T_m$ = 121 °C), but less so the dithiol form ($T_m$ = 113 °C), is stable at temperatures significantly higher than the growth temperature of *A. aeolicus* [ca. 90 °C (*13*)], it is probably vital for at least a fraction of the protein to remain in the former state in its cellular environment. Here again, the redox potential of the dithiol/disulfide must play an important role: while it may be expected to occur in the −100 to −250 mV range, it is also known that structurally important disulfide bridges have redox potentials near to or even below −400 mV (*75*). While such extreme values are unlikely in the case of *Aae* Fd1, since the disulfide bridge is reducible by DTT ($E° \sim -320$ mV), the disulfide bridge might nevertheless be relatively stable in the cytoplasm of *E. coli* [$E° \sim -260$ to −280 mV (*76*)]. However, even though recombinant *Aae* Fd1 is isolated with the disulfide bridge present, it remains to be determined whether this state is produced in the bacterial cells or, subsequently, during cell lysis and early fractionation steps.

Even regarding stability of hyperthermophilic proteins at large, *Aae* Fd1 appears to be an interesting exception, inasmuch as disulfide bonds are not currently listed among factors enhancing protein thermostability at high temperatures (*62*, *64*, *65*). Hyperthermophilic proteins are even known to contain lower percentages of cysteine than their thermophilic and mesophilic counterparts (*62*, *64*, *65*). The unique properties of *Aae* Fd1 also raise the issue of the rarity of hyperthermophilic plant-type Fds. It remains to be elucidated whether this occurrence results from structural constraints, making it more difficult for these proteins to reach the extremes of thermostability, or is merely a twist of Fd evolution.

## ACKNOWLEDGMENT

We thank Professor John L. Markley (University of Wisconsin) for providing the samples of human [2Fe-2S] ferredoxin and *Anabaena* 7120 vegetative [2Fe-2S] ferredoxin for comparative spectroscopic studies. We are indebted to Professor Keiichi Fukuyama (Osaka University) for sending the coordinates of the *E. coli* [2Fe-2S] ferredoxin. We also thank Drs. Robert Huber (Universität Regensburg, Germany) and Ronald Swanson (Diversa Corp., San Diego, CA) for providing us with *A. aeolicus* genomic DNA.

## REFERENCES

1. Beinert, H., Holm, R. H., and Münck, E. (1997) *Science 277*, 653−659.
2. Johnson, M. K. (1994) in *Encyclopedia of Inorganic Chemistry* (King, R. B., Ed.) Vol. 4, pp 1896−1915, Wiley, Chichester, U.K.
3. Yeh, A. P., Chatelet, C., Soltis, S. M., Kuhn, P., Meyer, J., and Rees, D. C. (2000) *J. Mol. Biol. 300*, 587−595.
4. Meyer, J. (2001) *FEBS Lett. 509*, 1−5.
5. Matsubara, H., and Saeki, K. (1992) *Adv. Inorg. Chem. 38*, 223−280.
6. Grinberg, A. V., Hannemann, F., Schiffler, B., Müller, J., Heinemann, U., and Bernhardt, R. (2000) *Proteins 40*, 590−612.
7. Jung, Y.-S., Gao-Sheridan, H. S., Christiansen, J., Dean, D. R., and Burgess, B. K. (1999) *J. Biol. Chem. 274*, 32402−32410.
8. Lange, H., Kaut, A., Kispal, G., and Lill, R. (2000) *Proc. Natl. Acad. Sci. U.S.A. 97*, 1050−1055.
9. Tokumoto, U., and Takahashi, Y. (2001) *J. Biochem. 130*, 63−71.
10. Barros, M. H., and Nobrega, F. G. (1999) *Gene 233*, 197−203.
11. Frolow, F., Harel, M., Sussman, J. L., Mevarech, M., and Shoham, M. (1996) *Nat. Struct. Biol. 3*, 452−458.
12. Klenk, H.-P., Clayton, R. A., Tomb, J.-F., White, O., Nelson, K. E., Ketchum, K. A., Dodson, R. J., Gwinn, M., Hickey, E. K., Peterson, J. D., Richardson, D. L., Kerlavage, A. R., Graham, D. E., Kyrpides, N. C., Fleischmann, R. D., Quackenbush, J., Lee, N. H., Sutton, G. G., Gill, S., Kirkness, E. F., Dougherty, B. A., McKenney, K., Adams, M. D., Loftus, B., Peterson, S., Reich, C. I., McNeil, L. K., Badger, J. H., Glodek, A., Zhou, L., Overbeek, R., Gocayne, J. D., Weidman, J. F., McDonald, L., Utterback, T., Cotton, M. D., Spriggs, T., Artiach, P., Kaine, B. P., Sykes, S. M., Sadow, P. W., D'Andrea, K. P., Bowman, C., Fujii, C., Garland, S. A., Mason, T. M., Olsen, G. J., Fraser, C. M., Smith, H. O., Woese, C. R., and Venter, J. C. (1997) *Nature 390*, 364−370.
13. Deckert, G., Warren, P. V., Gaasterland, T., Young, W. G., Lenox, A. L., Graham, D. E., Overbeek, R., Snead, M. A.,

Keller, M., Aujay, M., Huber, R., Feldman, R. A., Short, J. M., Olsen, G. J., and Swanson, R. V. (1998) *Nature 392*, 353−358.
14. Yoo, S.-J., Meyer, J., and Münck, E. (1999) *J. Am. Chem. Soc. 121*, 10450−10451.
15. Ausubel, F. M., Brent, R., Kingston, R. E., Moore, D. D., Seidman, J. G., Smith, J. A., and Struhl, K. (2001) *Current Protocols in Molecular Biology*, Wiley-Interscience, New York.
16. Tabor, S. (1990) in *Current Protocols in Molecular Biology* (Ausubel, F. M., Brent, R., Kingston, R. E., Moore, D. D., Seidman, J. G., Smith, J. A., and Struhl, K., Eds.) pp 16.2.1−16.2.11, Wiley-Interscience, New York.
17. Fujinaga, J., and Meyer, J. (1993) *Biochem. Biophys. Res. Commun. 192*, 1115−1122.
18. Golinelli, M.-P., Akin, L. A., Crouse, B. R., Johnson, M. K., and Meyer, J. (1996) *Biochemistry 35*, 8995−9002.
19. Xia, B., Jenk, D., LeMaster, D. M., Westler, W. M., and Markley, J. L. (2000) *Arch. Biochem. Biophys. 373*, 328−334.
20. Christiansen, J., Goodwin, P. J., Lanzilotta, W. N., Seefeldt, L. C., and Dean, D. R. (1998) *Biochemistry 37*, 12611−12623.
21. Lämmli, U. K. (1970) *Nature 227*, 680−685.
22. Habeeb, A. F. S. A. (1972) *Methods Enzymol. 25*, 457−464.
23. Quinkal, I., Davasse, V., Gaillard, J., and Moulis, J.-M. (1994) *Protein Eng. 7*, 681−687.
24. Johnson, M. K. (1988) in *Metal Clusters in Proteins* (Que, L., Jr., Ed.) ACS Symposium Series, Vol. 372, pp 326−342, American Chemical Society, Washington, DC.
25. Thomson, A. J., Cheesman, M. R., and George, S. J. (1993) *Methods Enzymol. 226*, 199−232.
26. Drozdzewski, P. M., and Johnson, M. K. (1988) *Appl. Spectrosc. 42*, 1575−1577.
27. Chatelet, C., Gaillard, J., Pétillot, Y., Louwagie, M., and Meyer, J. (1999) *Biochem. Biophys. Res. Commun. 261*, 885−889.
28. Thompson, J. D., Higgins, D. G., and Gibson, T. J. (1994) *Nucleic Acids Res. 22*, 4673−4680.
29. Page, R. D. M. (1996) *Comput. Appl. Biosci. 12*, 357−358.
30. Hugo, N., Armengaud, J., Gaillard, J., Timmis, K. N., and Jouanneau, Y. (1998) *J. Biol. Chem. 273*, 9622−9629.
31. Saeki, K., Suetsugu, Y., Tokuda, K.-I., Miyatake, Y., Young, D. A., Marrs, B. L., and Matsubara, H. (1991) *J. Biol. Chem. 266*, 12889−12895.
32. Armengaud, J., Meyer, C., and Jouanneau, Y. (1994) *Biochem. J. 300*, 413−418.
33. Jouanneau, Y., Meyer, C., Asso, M., Guigliarelli, B., and Willison, J. C. (2000) *Eur. J. Biochem. 267*, 780−787.
34. Meyer, J., Moulis, J.-M., and Lutz, M. (1986) *Biochim. Biophys. Acta 873*, 108−118.
35. Han, S., Czernuszewicz, R. S., Kimura, T., Adams, M. W. W., and Spiro, T. G. (1989) *J. Am. Chem. Soc. 111*, 3505−3511.
36. Han, S., Czernuszewicz, R. S., and Spiro, T. G. (1989) *J. Am. Chem. Soc. 111*, 3496−3504.
37. Fu, W., Drozdzewski, P. M., Davies, M. D., Sligar, S. G., and Johnson, M. K. (1992) *J. Biol. Chem. 267*, 15502−15510.
38. Gibson, J. F., Hall, D. O., Thornley, J. H. M., and Whatley, F. R. (1966) *Proc. Natl. Acad. Sci. U.S.A. 56*, 987−990.
39. Bertrand, P., and Gayda, J.-P. (1979) *Biochim. Biophys. Acta 579*, 107−121.
40. Werth, M. T., Cecchini, G., Manodori, A., Ackrell, B. A. C., Schröder, I., Gunsalus, R. P., and Johnson, M. K. (1990) *Proc. Natl. Acad. Sci. U.S.A. 87*, 8965−8969.
41. Thomson, A. J., Cammack, R., Hall, D. O., Rao, K. K., Briat, B., Rivoal, J. C., and Badoz, J. (1977) *Biochim. Biophys. Acta 493*, 132−141.
42. Tsibris, J. C. M., Tsai, R. L., Gunsalus, I. C., Orme-Johnson, W. H., Hansen, R. E., and Beinert, H. (1968) *Proc. Natl. Acad. Sci. U.S.A. 59*, 959−965.
43. Mukai, K., Kimura, T., Helbert, J., and Kevan, L. (1973) *Biochim. Biophys. Acta 295*, 49−61.
44. Ta, D. T., and Vickery, L. E. (1992) *J. Biol. Chem. 267*, 11120−11125.
45. Münck, E. (2000) in *Physical Methods in Bioinorganic Chemistry* (Que, L., Jr., Ed.) Chapter 6, University Science Books, Sausalito, CA.
46. Münck, E., Debrunner, P. G., Tsibris, J. C. M., and Gunsalus, I. C. (1972) *Biochemistry 11*, 855−863.
47. Dunham, W. R., Bearden, A. J., Salmeen, I. T., Palmer G., Sands, R. H., Orme-Johnson, W. H., and Beinert, H. (1971) *Biochim. Biophys. Acta 253*, 134−152.
48. Anderson, R. E., Dunham, W. R., Sands, R. H., Bearden, A. J., and Crespi, H. L. (1975) *Biochim. Biophys. Acta 408*, 306−318.
49. Lloyd, S. G., Franco, R., Moura, J. G., Moura, I., Ferreira, G. C., and Huynh, B. H. (1996) *J. Am. Chem. Soc. 118*, 9892−9900.
50. Achim, C., Bominaar, E. L., Meyer, J., Peterson, J., and Münck, E. (1999) *J. Am. Chem. Soc. 121*, 3704−3714.
51. Rao, K. K., Cammack, R., Hall, D. O., and Johnson, C. E. (1971) *Biochem. J. 122*, 257−265.
52. Kissinger, C. R., Sieker, L. C., Adman, E. T., and Jensen, L. H. (1991) *J. Mol. Biol. 219*, 693−715.
53. Macedo, A. L., Moura, I., Surerus, K. K., Papaefthymiou, V., Liu, M. Y., LeGall, J., Münck, E., and Moura J. J. (1994) *J. Biol. Chem. 269*, 8052−8058.
54. Gorst, C. M., Zhou, Z. H., Ma, K., Teng, Q., Howard, J. B., Adams, M. W. W., and La Mar, G. N. (1995) *Biochemistry 34*, 8788−8795.
55. Lelong, C., Sétif, P., Bottin, H., André, F., and Neumann, J.-M. (1995) *Biochemistry 34*, 14462−14473.
56. Macedo-Ribeiro, S., Darimont, B., Sterner, R., and Huber, R. (1996) *Structure 4*, 1291−1301.
57. Privalov, P. L., and Potekhin, S. A. (1986) *Methods Enzymol. 131*, 4−51.
58. Moczygemba, C., Guidry, J., Jones, K. L., Gomes, C. M., Teixeira, M., and Wittung-Stafshede, P. (2001) *Protein Sci. 10*, 1539−1548.
59. Wittung-Stafshede, P., Gomes, C. M., and Teixeira, M. (2000) *J. Inorg. Biochem. 78*, 35−41.
60. La−Rosa, C., Milardo, D., Grasso, D., Guzzi, R., and Sprotelli, L. (1995) *J. Phys. Chem. 99*, 14864−14870.
61. Kakuta, Y., Horio, T., Takahashi, Y., and Fukuyama, K. (2001) *Biochemistry 40*, 11007−11012.
62. Cambillau, C., and Claverie, J.-M. (2000) *J. Biol. Chem. 275*, 32383−32386.
63. Chan, M. K., Mukund, S., Kletzin, A., Adams, M. W. W., and Rees, D. C. (1995) *Science 267*, 1463−1469.
64. Kumar, S., Tsai, C.-J., and Nussinov, R. (2000) *Protein Eng. 13*, 179−191.
65. Szilágyi, A., and Závodszky, P. (2000) *Structure 8*, 493−504.
66. Karshikoff, A., and Ladenstein, R. (2001) *Trends Biochem. Sci. 26*, 550−556.
67. Macedo-Ribeiro, S., Martins, B. M., Barbosa Pereira, P. J., Buse, G., Huber, R., and Soulimane, T. (2001) *J. Biol. Inorg. Chem. 6*, 663−674.
68. Wu, C.-K., Dailey, H. A., Rose, J. P., Burden, A., Sellers, V. M., and Wang, B.-C. (2001) *Nat. Struct. Biol. 8*, 156−160.
69. Morales, R., Charon, M.-H., Hudry-Clergeon, G., Pétillot, Y., Nørager, S., Medina, M., and Frey, M. (1999) *Biochemistry 38*, 15764−15773.
70. Webba da Silva, M., Sham, S., Gorst, C. M., Calzolai, L., Brereton, P. S., Adams, M. W. W., and La Mar, G. N. (2001) *Biochemistry 40*, 12575−12583.
71. Wang, P.-L., Donaire, A., Zhou, Z. H., Adams, M. W. W., and La Mar, G. N. (1996) *Biochemistry 35*, 11319−11328.
72. Sayle, R. A., and Milner-White, E. J. (1995) *Trends Biochem. Sci. 20*, 374−376.
73. Pfeil, W., Gesierich, U., Kleemann, G. R., and Sterner, R. (1997) *J. Mol. Biol. 272*, 591−596.
74. Hatanaka, H., Tanimura, R., Katoh, S., and Inagaki, F. (1997) *J. Mol. Biol. 268*, 922−933.
75. Gilbert, H. F. (1995) *Methods Enzymol. 251*, 8−28.
76. Ritz, D., and Beckwith, J. (2001) *Annu. Rev. Microbiol. 55*, 21−48.

BI015981M